ChemComm

COMMUNICATION

View Article Online
View Journal | View Issue

Cite this: *Chem. Commun.*, 2015, **51**, 12365

Received 13th May 2015,
Accepted 4th June 2015

DOI: 10.1039/c5cc03981a

www.rsc.org/chemcomm

Graphene quantum dot-doped polyaniline nanofiber as high performance supercapacitor electrode materials†

Sanjoy Mondal, Utpal Rana and Sudip Malik*

Graphene quantum dot-doped polyaniline composites have been prepared by the chemical oxidation of aniline. Synthesized novel fibrous composites show an excellent specific capacitance value of ~1044 F g^{-1} at a current density of 1 A g^{-1} as well as moderate cyclic stability with a retention of life time of 80.1% after 3000 cycles.

Supercapacitors or electrochemical capacitors have received great attention in recent years due to a strong demand for lightweight and flexible portable energy storage devices.[1–5] Supercapacitors are quite different from traditional capacitors. They combine the advantages of dielectric capacitors and rechargeable batteries to achieve high power density, long durability, fast charge–discharge rate and operational safety. A good supercapacitor material should exhibit high power density, long cycle life, and fast charge–discharge capability. During the last decade, different materials like metal oxides,[6] carbon materials (CNT or graphene),[7,8] conducting polymers,[9] and composite materials[10] have been reported as supercapacitor electrode materials. Among different conducting polymers, polyaniline (PANI) is the most important and popular polymer due to its easy synthesis, low cost of starting or raw materials, good environmental and thermal stability, multiple redox states, high range electrical conductivity *etc.*[11] Because of these advantages, bulk PANI is also applied in supercapacitor electrode substances.[9,10,12,13,14] Recent developments of facile as well as effective methods of synthesis of PANI nanotubes with high aspect ratio and increased surface area have generated tremendous interest as capacitors.

Owing to their exciting properties such as high electrical conductivity, high surface area, tunable photoluminescence and excellent dispersion in various solvents, graphene quantum dots (GQDs) have emerged as promising materials for energy storage devices, bioimaging devices and fuel cells.[15] The excellent properties of GQDs and the advantages of PANI have received more attention for preparation of high performance supercapacitor electrode materials.[8b,c,16] Recently, there were some reports of supercapacitors based on polyaniline nanostructure made either by electro-spinning[17] or by electrochemical deposition of PANI on a ZnO template.[18] In this context, our aim is to prepare high performance supercapacitor electrode materials exploiting the possible synergy of GQD and PANI (Scheme 1).

GQDs were prepared from graphene oxide according to the reported procedure.[19] Synthesized GQDs were unambiguously characterized with the help of available techniques. In UV-vis study (Fig. S1, ESI†), the peak at 198 nm was for the π–π* transition of C=C within the GQD structure. The fluorescence emission peaks of the GQDs showed the bathochromic shift with increasing the excitation wavelength and maximum fluorescence intensity was observed at the excited wavelength of 420 nm (Fig. 1a).[19] Water-dispersed GQD solution produced sky-blue fluorescence (inset image of Fig. 1a) under a UV lamp (365 nm). A dynamic light scattering study provided the narrow lateral size distribution of GQDs ranging from 4.0 to 8.0 nm (Fig. 1b). AFM (Fig. 1c) and TEM images (Fig. 1d) exhibited homogenous GQDs having a size of ~6.0 nm and a narrow height distribution from 0.6 to 3.1 nm (1.4 nm average thickness), signifying that the GQDs typically consisted of 1–5 graphene layers. All these observations indicated the formation of GQDs having

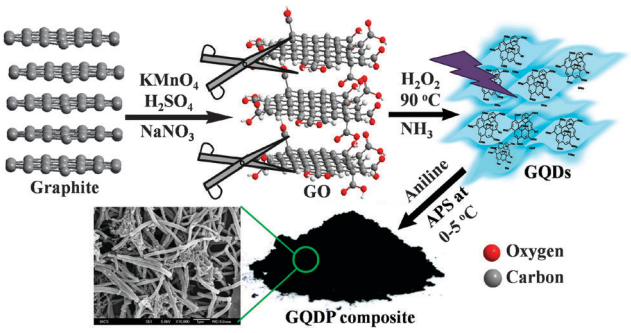

Scheme 1 Schematic diagram for the preparation of GQDP composites.

Polymer Science Unit, Indian Association for the Cultivation of Science, 2A & 2B Raja S.C. Mullick Road., Jadavpur, Kolkata – 700032, India. E-mail: psusm2@iacs.res.in

† Electronic supplementary information (ESI) available: Preparation of GO, GQD; characterization UV, PL, XRD, FTIR, Raman, CV and impedance data for GQD and GQDP composites. See DOI: 10.1039/c5cc03981a

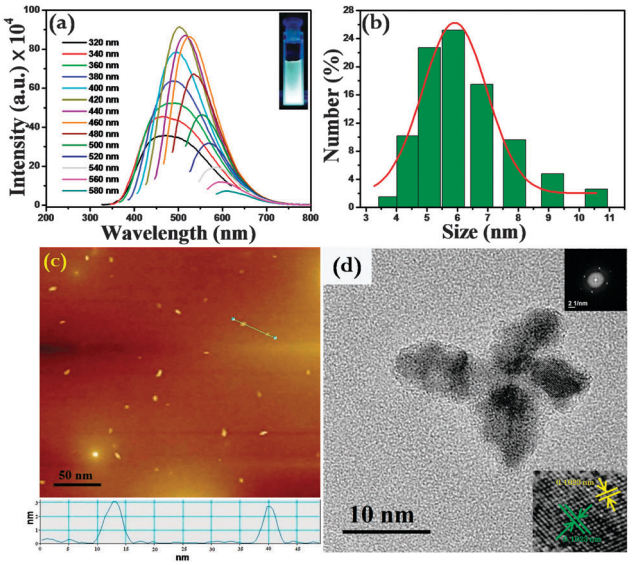

Fig. 1 Characterization data of synthesized graphene quantum dots (a) PL study with different excitation wavelengths, inset picture shows digital image GQD under UV lamp (365 nm), (b) dynamic light scattering, (c) AFM study on mica surface with particles size ~6 nm, (d) TEM image with particles size ~6 nm (inset diffraction and fringe pattern).

particles size ~6.0 nm. Synthesized GQDs were used as a dopant and soft template for the preparation of five different GQD–PANI (GQDP) composites.

Typically, a requisite amount of GQDs (weight %) was dispersed in water (Table S1, ESI†), and 100 mg (100 μL, 1.1 mmol) of aniline was added to it with constant stirring for one hour at room temperature (25 °C). The reaction mixture was cooled to 10 °C and an aqueous solution of APS (250 mg, 1.1 mmol) was added slowly. The resulting mixture was allowed to stand at 5 °C temperature for 24 h. The deep green coloured precipitate was washed with water followed by methanol and acetone several times to remove the oligomers and excess APS. Finally, the product was dried at room temperature in a vacuum for 24 h to get GQDP composites with ~85% yield.

All GQDP composites reveal one dimensional (1D) nanofibers of different diameters and several micrometers in length, except GQDP0 and GQDP20 (Fig. 2). The diameter of the PANI nanofibers increases with the increase of wt% GQD from GQDP5 to GQDP10 and it decreases from GQDP15 to GQDP20 (Table 1). In the case of GQDP20 agglomerated structures are formed and homogeneous polymerization does not possibly take place at higher concentration of GQDs. Interestingly, high aspect ratio nanofibers with uniform diameter are observed for GQDP10. Nanofibers with rougher surfaces are formed in all cases and it will enhance the accessible surface area and speed up the ion diffusion process, indicating the suitability of GQDP as supercapacitor electrode materials.

In the HRTEM image (Fig. 3), all composites show fibre like morphology with different aspect ratio depending on the GQD to aniline w/w ratio. In the GQDP20 composite, small or damaged fibers are formed. A closer look at the HRTEM images of GQDPs (inset image of Fig. 3) reveals that the clear contrast

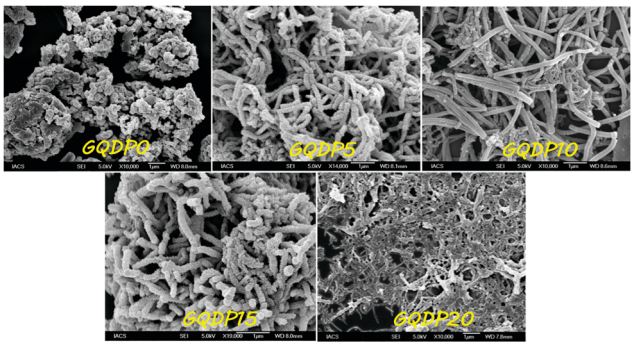

Fig. 2 FESEM images of synthesized GQDP composites having different aniline to GQDs (w/w) ratios.

Table 1 Diameter and specific capacitance of GQDP composites

Composites	SEM (OD)	TEM (OD)	TEM (ID)	Sp. capacitance[a] (F g^{-1})
GQDP0	Agglomerate	Agglomerate	—	205.7
GQDP5	182 nm	184 nm	—	332.8
GQDP10	194 nm	195 nm	94 nm	1044.3
GQDP15	190 nm	187 nm	14 nm	776.3
GQDP20	67 nm	63 nm	—	319.3

[a] All GCD at 1 A g^{-1} current density, OD/ID = outer/inner diameter.

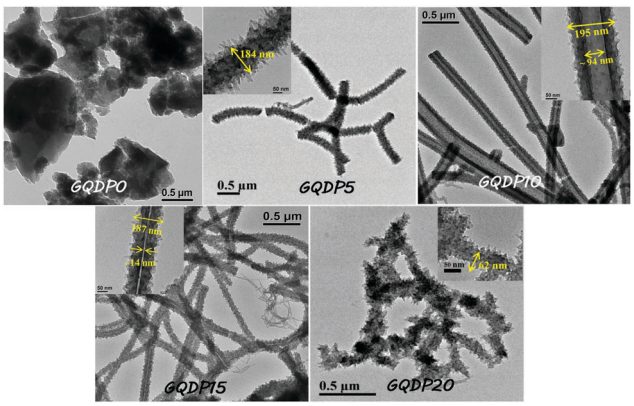

Fig. 3 HRTEM images of different GQDP composites having different aniline to GQD w/w ratios with different inner and outer diameters.

between the edge and the central part of fiber in the case of GQDP10 and GQDP15 nanofibers is suggestive of the formation of nanotubes. Interestingly, a maximum inner diameter (~94 nm) with ~50 nm wall thickness is observed for GQDP10 resulting in the higher surface area among five composites. Without GQD, random structures of PANI are always observed, indicating that the presence of GQD during the polymerization is essential to get nanofibers of PANI.

In the UV-vis studies of GQDPs (Fig. 4), three absorbance peaks at 362 nm (π → π* transition), 438 nm (polaron → π* transition) and 900 nm (π → polaron transition) with an extended free tail to the IR region reveal the presence of the emeraldine salt state of PANI chains in the composite.[11] Typical FTIR stretching bands (Fig. S3, ESI†) at 3432, 1580, 1496, 1300, 1140 and 800 cm^{-1} for γN–H, γC=C of quinoid rings, benzenoid rings,

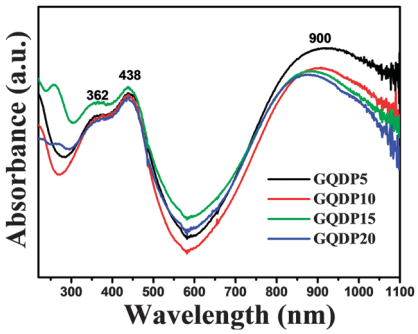

Fig. 4 UV-vis spectra of synthesized GQDP composites in aqueous medium.

γC–N, secondary aromatic amine, aromatic in-plane and out-of-plane deformation of 1,4-disubstituted benzene, respectively prove the PANI formation.[11,20] Disappearance of the –COOH stretching band (1724 cm^{-1}) in GQDP composites reflects the involvement of GQDs in composite formation. XPS studies have been further performed to characterize the chemical environment of the GQDP composite (Fig. S4, ESI†). Three peaks at ~285, 400 and 532.5 eV correspond to C1s, N1s and O1s, respectively. A deeper insight into the XPS spectrum in the region of 391–408 eV (N1s of PANI) has revealed three sub-peaks at ~389.6 eV (–N═), 399.3 eV (–NH–) and 400.2 eV (–N+–) (Fig. S4b, ESI†).[21] Functional groups and chemical bonds (C═C, C–C, C═O, C–OH *etc.*) are also observed through the deconvolution XPS study of O1s and C1s (Fig. S4c and d, ESI†). The XRD pattern of the synthesized GO shows a strong signal at $2\theta = 11.24^\circ$ and 26.71° for multilayer graphite[22] and the position of the peak at 11.24° is shifted to $2\theta = 8.61^\circ$ in GQDs (Fig. S2, ESI†). Powder XRD patterns of the GQDP composite (Fig. S5, ESI†) provide information about the slight crystalline nature as well as the interaction of GQDs with PANI in the composites.[23] The peaks at $2\theta = 20.3^\circ$ (100) and 25.5° (110) are for periodicity in the parallel and perpendicular directions to the PANI chains, respectively.[24]

GQDP nanotubes having high aspect ratio as well as the enhanced surface-to-volume ratio are expected to become a new promising material for energy storage applications. Capacitive performances of five GQDPs have been evaluated by cyclic voltammetry (CV) and galvanostatic charge–discharge methods with three electrode systems. Two pairs of characteristic redox peaks of PANI (Fig. 5a) are observed for all GQDP composites.[25] The large area under the CV curve represents the good capacitance value. Highest CV currents with two pairs of redox peaks of GQDP10 indicate the high conductivity or low internal resistance of this composite than other GQDP composites, as the electrode material. CV curves of GQDP10 at different scan rates (Fig. S7, ESI†) exhibit well-resolved as well as reversible redox peaks at lower scan rate. With increasing scan rate, peak current increases with broadening of CV peaks, signifying the pseudocapacitance feature of GQDP. The asymmetric nature of the CV curve suggests the combined double-layer and pseudocapacitive contributions to the total capacitance. Strong electrochemical capacitance properties of the GQDP composites are further tested by the galvanostatic charge–discharge (GCD) method at current density 1 A g^{-1}. All GCD curves produce a

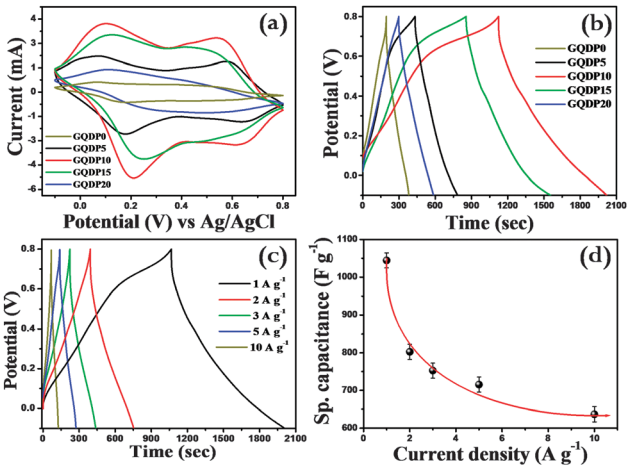

Fig. 5 (a) CV study of GQDP composites at the scan rate of 100 mV s^{-1}; (b) GCD curve of GQDP composites at 1 A g^{-1} current density; (c) GCD curve at different current densities and (d) specific capacitance *vs.* current density plot of the GQDP10 composite. All experiments in 0.5 M H_2SO_4 electrolyte solution.

triangle type shape and high reversibility of the GQDP nanomaterials during the charge–discharge process (Fig. 5b). The synthesized GQDP composites show a very small voltage drop (0.035 V) during charge–discharge processes, which is another criterion for good supercapacitor materials.

Specific capacitance (C_s) values are also calculated from the GCD curve using the following equation:

$$C_s = \frac{i \times \Delta t}{\Delta V \times m} (\mathrm{F\ g^{-1}})$$

Where, 'i' = current (A); 'Δt' = discharge time (s), 'ΔV' = voltage windows (V) and 'm' = mass of GQDP composites (g).[26,27]

The calculated specific capacitance values of GQDP0, GQDP5, GQDP10, GQDP15 and GQDP20 composites are 206, 333, 1044, 776 and 319 F g^{-1} respectively. The maximum specific capacitance (1044 F g^{-1}) is achieved for the GQDP10 composite because higher surface areas in nanotube morphology provide better conductive paths for fast electron transport. All GCD curves show typical nonlinear behaviour that confirms a pseudo-capacitive nature.[28] The specific capacitance value decreases with increasing current density (Fig. 5c and d). The specific capacitance of GQDP10 observed at the current densities of 1, 2, 3, 5 and 10 A g^{-1} are 1044, 802, 752 and 635 F g^{-1}, respectively. The maximum energy density (E) and power density (P) estimated for the GQDP10 composite are 117.45 W h kg^{-1} and 448.8 W kg^{-1}, respectively.

The cyclic stability is also an imperative parameter from the application point of view. Long term cyclic life stability has been tested by 3000 continuous GCD for GQDP10 composite. After the 3000th cycle, 19.9% of total specific capacitance loss (*i.e.* ~80.1% retention of specific capacitance) at current density 1 A g^{-1} in 0.5 M H_2SO_4 electrolyte solution (Fig. 6) has been observed. This decrease of specific capacitance after 3000 cycles may be explained by the loss of active material in the current collector (due to swelling or contraction) which causes the partial blockage of the regular structure.

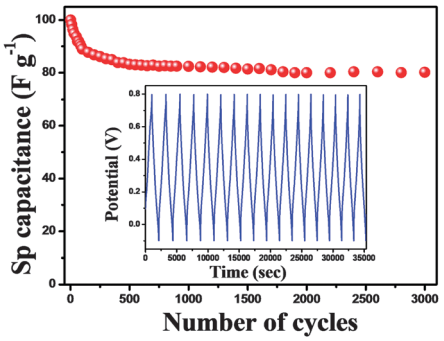

Fig. 6 3000 charge–discharge cycle life stability of GQDP10 composite, inset GCD curve for 10 consecutive cycles.

In conclusion, we have successfully synthesized ~6.0 nm size graphene quantum dots from graphene oxide flakes. The synthesized GQDP composites are nanofibrous or nanotubular in nature. The inner diameter of GQDP nanotubes varies with the ratio (w/w) of GQD to aniline. The synthesized GQDP composites show a highest specific capacitance value of ~1044 F g^{-1} at the current density of 1 A g^{-1} with 80.1% retention of capacitance after 3000 cycles.

Dr Malik acknowledges CSIR, INDIA (project no. 02(0161)/13/EMR-II) for the financial support. S. Mondal is acknowledge CSIR, New Delhi, India for the fellowship.

Notes and references

1 M. D. Stoller, S. Park, Y. Zhu, J. An and R. S. Ruoff, *Nano Lett.*, 2008, **8**, 3498.
2 M. Winter and R. J. Brodd, *Chem. Rev.*, 2004, **104**, 4245.
3 C. Liu, F. Li, L. P. Ma and H. M. Cheng, *Adv. Mater.*, 2010, **22**, E28.
4 X. Huang, X. Qi, F. Boey and H. Zhang, *Chem. Soc. Rev.*, 2012, **41**, 666.
5 H. P. Cong, X. C. Ren, P. Wang and S. H. Yu, *Energy Environ. Sci.*, 2013, **6**, 1185.
6 J. Jiang, Y. Li, J. Liu, X. Huang, C. Yuan and X. W. Lou, *Adv. Mater.*, 2012, **24**, 5166.
7 (*a*) L. L. Zhang and X. S. Zhao, *Chem. Soc. Rev.*, 2009, **38**, 2520; (*b*) M. Kaempgen, C. K. Chan, J. Ma, Y. Cui and G. Gruner, *Nano Lett.*, 2009, **9**, 1872.
8 (*a*) D. N. Futaba, K. Hata, T. Yamada, T. Hiraokal, Y. Hayamizu, Y. Kakudate, O. Tanaike, H. Hatori, M. Yumura and S. Iijima, *Nat. Mater.*, 2006, **5**, 987; (*b*) X. Zang, X. Li, M. Zhu, X. Li, Z. Zhen, Y. He, K. Wang, J. Wei, F. Kang and H. Zhu, *Nanoscale*, 2015, **7**, 7318; (*c*) X. Zang, M. Zhu, X. Li, X. Li, Z. Zhen, J. Lao, K. Wang, F. Kang, B. Wei and H. Zhu, *Nano Energy*, 2015, **15**, 83.
9 (*a*) Y. Miao, W. Fan, D. Chen and T. Liu, *ACS Appl. Mater. Interfaces*, 2013, **5**, 4423; (*b*) X. Li, L. Yang, Y. Lei, L. Gu and D. Xiao, *ACS Appl. Mater. Interfaces*, 2014, **6**, 19978.
10 (*a*) L. Wang, X. Lu, S. Lei and Y. Song, *J. Mater. Chem. A*, 2014, **2**, 4491; (*b*) Q. Zhou, Y. Li, L. Huang, C. Li and G. Shi, *J. Mater. Chem. A*, 2014, **2**, 17489.
11 (*a*) U. Rana and S. Malik, *Chem. Commun.*, 2012, **48**, 10862; (*b*) U. Rana, K. Chakrabarti and S. Malik, *J. Mater. Chem.*, 2012, **22**, 15665; (*c*) S. Mondal, U. Rana and S. Malik, *ACS Appl. Mater. Interfaces*, 2015, **7**, 10457.
12 (*a*) S. H. Domingues, R. V. Salvatierra, M. M. Oliveira and A. J. G. Zarbin, *Chem. Commun.*, 2011, **47**, 2592; (*b*) X. Yan, Z. Tai, J. Chen and Q. Xue, *Nanoscale*, 2011, **3**, 212.
13 W. Chen, R. B. Rakhi and H. N. Alshareef, *Nanoscale*, 2013, **5**, 4134.
14 Z. Lei, Z. Chen and X. S. Zhao, *J. Phys. Chem. C*, 2010, **114**, 19867.
15 M. Bacon, S. J. Bradley and T. Nann, *Part. Part. Syst. Charact.*, 2014, **31**, 415.
16 W. Liu, X. Yan, J. Chen, Y. Feng and Q. Xue, *Nanoscale*, 2013, **5**, 6053.
17 Y. E. Miao, W. Fan, D. Chen and T. Liu, *ACS Appl. Mater. Interfaces*, 2013, **5**, 4423.
18 Z. L. Wang, R. Guo, G. R. Li, H. L. Lu, Z. Q. Liu, F. M. Xiao, M. Zhang and Y. X. Tong, *J. Mater. Chem.*, 2012, **22**, 2401.
19 F. Jiang, D. Chen, R. Li, Y. Wang, G. Zhang, S. Li, J. Zheng, N. Huang, Y. Gu, C. Wang and C. Shu, *Nanoscale*, 2013, **5**, 1137.
20 B. A. Deore, I. Yu and M. S. Freund, *J. Am. Chem. Soc.*, 2004, **126**, 52.
21 K. Lee, S. Cho, S. H. Park, A. J. Heeger, C. W. Lee and S. H. Lee, *Nature*, 2006, **441**, 65.
22 N. Wu, X. She, D. Yang, X. Wu, F. Su and Y. Chen, *J. Mater. Chem.*, 2012, **22**, 17254.
23 G. Wang, X. Shen, B. Wang, J. Yao and J. Park, *Carbon*, 2009, **47**, 1359.
24 L. Shi, R. Liang and J. Qiu, *J. Mater. Chem.*, 2012, **22**, 17196.
25 H. Wang, Q. Hao, X. Yang, L. Lu and X. Wang, *Nanoscale*, 2010, **2**, 2164.
26 D. Ghosh, S. Giri and C. K. Das, *Nanoscale*, 2013, **5**, 10428.
27 X. Yan, Z. Tai, J. Chen and Q. Xue, *Nanoscale*, 2011, **3**, 212.
28 X. Ma, Y. Li, Z. Wen, F. Gao, C. Liang and R. Che, *ACS Appl. Mater. Interfaces*, 2015, **7**, 974.

